

# Optimization- and Rule-Based Energy Management Systems at the Canadian Renewable Energy Laboratory Microgrid Facility

Mauricio Restrepo<sup>d</sup>, Claudio A. Cañizares<sup>a,\*</sup>, John W. Simpson-Porco<sup>b</sup>, Peter Su<sup>c</sup>, John Taruc<sup>c</sup>

<sup>a</sup>*Department of Electrical and Computer Engineering, University of Waterloo, Waterloo, ON N2L 3G1, Canada*

<sup>b</sup>*Department of Electrical and Computer Engineering, University of Toronto, Toronto, ON M5S 3G4, Canada*

<sup>c</sup>*Canadian Solar Inc., 545 Speedvale Avenue West, Guelph, ON N1K 1E6, Canada*

<sup>d</sup>*Department of Electrical and Electronics Engineering, Universidad del Norte, Barranquilla, 081007, Colombia*

---

## Abstract

This paper presents the development, implementation, and commissioning of two different Energy Management Systems (EMSs) for the Canadian Renewable Energy Laboratory (CANREL), a microgrid testbed located in Guelph, ON, Canada, for the existing hardware, software, and communication infrastructure, which constrained the implementation options. A Rule-based EMS (RBEMS), which is typically found in microgrid controllers nowadays, and an implementation of an Optimization-based EMS (OBEMS), which is not usual in today's controllers, are proposed, tested, and demonstrated in the microgrid testbed. The RBEMS consists of a state machine that represents the commitment of different genset units in the system and the curtailment of load and renewable generation. The OBEMS is based on a unit commitment model for microgrids that minimizes the generation and curtailment costs, while operating the microgrid equipment according to technical limits. Both EMS systems are integrated into a Python application which integrates various open-source packages and solvers, making it affordable, flexible and easy to replicate and upgrade. The successful implementation and performance of the EMSs is discussed, showing that the components of the microgrid follow the dispatch commands, with the OBEMS yielding better overall results than the RBEMS, as expected, using the existing communications links and maintaining the stability of the microgrid.

*Keywords:* Energy Management System (EMS), testbed, microgrids, open source, optimization, state machine

---

## 1. Introduction

Microgrids have been shown to efficiently integrate distributed generation resources and loads, using centralized and decentralized controls that compensate the variability of renewables to maintain system stability. Initially conceived for operation in remote areas and military facilities, the applications of microgrids are numerous today in universities, factories, and commercial building. New microgrid developments are being built around the world as the capital costs of renewable generation and storage technologies continue to drop [1]; from 2015 to 2018, the number of identified microgrid projects has grown 57.13% from 1437 to 2258, and total installed capacity has grown 31.55%, from 13400 MW to 19575 MW [2, 3].

The growing use of microgrids as a vehicle to integrate distributed energy resources involves the use of controllers with integrated Energy Management Systems (EMSs) for proper asset management and efficient system operation.

There are two main categories of EMSs: Rule-based EMS (RBEMS) and Optimization-based EMS (OBEMS). A RBEMS allocates the resources of the microgrid using predefined logical rules so that the energy produced by renewable resources can be adequately delivered or stored. An OBEMS is more sophisticated, and usually implements an optimization-based Unit Commitment (UC) model that considers several technical constraints while minimizing the operation costs.

Testing the performance of such systems under close-to-real-life conditions to identify stability and communication issues becomes very important, before wide-spread deployment of these controllers commences. Such testing is usually performed with Real Time Simulators (RTSs) and/or physical simulation testbeds [4]. The former can simulate the real-time electrical behaviour of power systems, and interface with external controllers and protection devices to verify their performance under realistic conditions, whereas the latter includes real generation and storage systems, load banks, and controllable inverters to simulate the actual behaviour of a microgrid under different conditions and to also test external controllers and protection devices.

Examples of RTSs that are used to test EMSs are found in [5, 6, 7, 8, 9]. These works use these simulators to model

---

\*Corresponding author

Email addresses: mauricioestrepo@uninorte.edu.co

(Mauricio Restrepo), ccanizares@uwaterloo.ca

(Claudio A. Cañizares), jwsimpson@ece.utoronto.ca (John W. Simpson-Porco), peter.su@canadiansolar.com (Peter Su),

john.taruc@canadiansolar.com (John Taruc)

## Nomenclature

### Sets

$\mathcal{T}_t$  Set of prediction steps at time  $t$

### Sub- and Super-Indices

$-,_-$  Maximum and minimum limit

$b$  Battery

$cur$  Curtailment

$d$  Diesel genset unit

$gen$  Generation

$in$  Input (charging)

$k_t$  Prediction step at time  $t$

$lb$  Load bank

$out$  Output (discharging)

$pvs$  PV simulator

$ws$  Wind simulator

### Parameters

$\Delta t_{k_t}$  Time interval at step  $k_t$  [h]

$\eta$  Battery efficiency

$a_g, b_g$  Linear and constant term factors of diesel genset's cost function [\$/kWh, \$/h]

$C^{cur}$  Curtailment costs [\$/kWh]

$C^{sup}, C^{sdn}$  Start-up and shut-down costs [\$]

$M_{dn}$  Minimum down time [h]

$M_{up}$  Minimum up time [h]

$P_{lb}$  Active power demand of load bank [p.u.]

$P_{pvs}$  Active power output of PV simulator [p.u.]

$P_{ws}$  Active power output of wind simulator [p.u.]

$R_{dn}$  Maximum ramp down [p.u./h]

$R_{up}$  Maximum ramp up [p.u./h]

$Rs$  Reserve factor [%]

$t$  Input update time [s]

### Variables

$Drt$  Diesel runtime

$Gcur$  Generation curtailment signal

$J$  Objective variable

$KD$  Diesel genset dispatch factor

$Lcur$  Load curtailment signal

$P$  Active power output of generation units [p.u.]

$SoC$  State of charge [%]

$U$  Start-up decision variable (1=ON)

$V$  Shut-down decision variable (1=OFF)

$W$  Unit commitment decision variable (1=ON, 0=OFF)

the operation of ac and dc microgrids, but the studies that are carried out and the interfaces with external devices vary. In [5], a RTS is used to study the performance of external controllers and protection systems for several operating conditions of a microgrid, including faults, load restoration, resynchronization, and islanding. The performance of an external EMS controller for a grid-connected microgrid that includes diesel gensets and batteries is studied through a RTS in [6], and similar studies for an industrial microgrid, considering operation conditions such as generation trip and load shedding, are presented in [7]. The authors in [8] conduct microgrid design and technical feasibility studies using a RTS to test all the SCADA hardware and software, and the PLCs to be deployed in the actual microgrid. Additionally, [9] proposes to interface a RTS with fast FPGAs that emulate the dynamic behavior of PV and battery inverters, in order to test EMS controllers and physical relays under fault conditions. The RTS tools presented in these papers show an adequate representation of different elements of the microgrid; however, in many cases, communication elements are not accurately represented, and sometimes these simulators do not sup-

port power electronics converters with high switching frequencies [10], which are important to test the performance of actual microgrid controllers.

In contrast, several physical testbed facilities have been created to assess various technical aspects of microgrids, as has been thoroughly documented in [11] and [12]. However, few studies have been published on the use of physical microgrid testbeds to discuss the implementation and evaluate the performance of EMSs. Of particular relevance are [13] and [14], which report the experimental testing of real-time EMSs in a local day-ahead energy framework for isolated microgrids on the microgrid testbed of the Catalonia Institute for Energy Research (IREC). These papers include a RBEMS with no optimization [13], which are typically found in today's controllers, and a Mixed-integer Nonlinear Programming (MINLP) OBEMS model that is solved using an interior-point method [14], which are unusual in present commercial controllers. A full-scale microgrid demonstration project in Dongao island, China, for testing a RBEMS, is presented in [15], where rules are designed to maintain enough reserves in the system to serve the load by committing two diesel genset units, connecting

four wind turbines, and charging and discharging a battery bank. Moreover, [16] depicts the testing of a Model Predictive Control (MPC) approach for an OBEMS in a physical microgrid testbed located in Athens, Greece, under different look-ahead windows. This control strategy is also used in [17], where an MPC method with an OBEMS is implemented for controlling active and reactive power outputs of several generation assets at the University of Genova - Savona Campus' microgrid, which includes microturbines, boilers, chillers, PV arrays, and energy storage systems. In [18], an actual microgrid testbed at the University of Melbourne, consisting of a battery bank, a solar PV emulator, and a gasoline genset, is used to test a two-layer, hierarchical, MPC-based microgrid control strategy, which optimizes simultaneously the fuel consumption of the genset, and the thermal performance of the battery. Although these works tested different EMS models under close to real conditions, they did not compare and contrast the performance of RBEMS and OBEMS.

Another important aspect of microgrid EMS implementation is the performance of communication protocols to control and supervise grid components. These protocols should provide simplicity and enough security to allow the efficient interchange of data among controllers, generators, loads, and measurement devices. In this context, Internet of Things (IoT) protocols such as MQTT, AMQP or DDS have shown potential in various microgrid applications, since they are conceived to interconnect numerous devices with small payload and low energy consumption [19]. In [20], a two-level IoT platform based on Modbus and MQTT protocols is proposed to dynamically compensate for neutral currents in unbalanced multi-microgrid systems, showing a negligible effect of communication delays in the proposed controller performance. This work is related to [21], in which a similar communication platform is used to analyze an EMS in a multi-microgrid system, studying the effects of centralized communication delays, and proposing distributed control and communication approaches when the connection with the central controller fails. Moreover, authors in [22] present a microgrid communication scheme based on the DDS protocol and demonstrate its performance for microgrid islanding and resynchronization, showing maximum delays between 7 to 9 cycles in state changes. For EMS implementations, in which message delays are not as critical as in protection or resynchronization, the MQTT protocol used in this work is appropriate, due to its simplicity, low overhead, and good performance in constrained networks [19].

In summary, there are few reported comprehensive studies of general and practical EMS implementations, and there is a large gap in the literature regarding testing and comparison of EMSs on a full-scale physical testbed. The latter is particularly important for validating the interactions of controllers, communication networks, Distributed Generators (DGs), and power electronics converters. Moreover, to the best of the authors' knowledge, there are very few works, such as [23, 24], that report the devel-

opment and implementation of EMS controllers based on open-source programming tools, optimization solvers, and communication protocols, which are important for facilitating further wide-spread deployment of microgrid technologies.

Based on these identified gaps, the objective of this paper is to present the practical implementation, testing, and comparison of a RBEMS and an OBEMS for isolated operation at the Canadian Renewable Energy Laboratory (CANREL), an existing microgrid testing facility in Guelph, ON, Canada. As is the case with many commissioned facilities, the existing hardware, software, and communication infrastructure cannot be modified, and any external EMS systems must be designed to interface with the existing software and communication protocols. This is a scenario of significant practical relevance, and constrains the design possibilities relative to a new microgrid deployment. Our implementations use open source software to interact with the existing control and communication layers, and we demonstrate implementations of two different and well-known EMS approaches: rule-based EMS and optimization-based EMSs. It should be mentioned that no new EMS algorithms nor uncertainty management is investigated. Instead, our focus in this paper is on the challenges one encounters when implementing and testing popular EMSs in a real commissioned microgrid testbed. This addresses a gap in the literature of lack of verification of EMS systems under realistic deployment conditions. Moreover, this work provides insight into the operational, communication, and computational issues associated with EMS real implementations that cannot be discerned through simulation studies. Thus, the main contributions of this paper are as follows:

- Demonstrate the feasibility of using open source programming languages, optimization solvers and communication protocols, with an existing and inflexible hardware, software, and communication infrastructure, as a proof of concept for the practical development of EMS controllers.
- Develop and compare two different EMS methods, and illustrate their testing under different load and generation conditions. In particular, our presentation highlights computation and communication issues that must be considered for actual implementations.

The paper is organized as follows: Section 2 discusses EMS for microgrids, particularly the general elements of previous rule-based and optimization-based algorithms, and describes the main characteristics of the CANREL microgrid facility. Section 3 presents the EMS algorithms developed in this work, and the implementation process in Python for the testbed. The simulation results are presented and discussed in Section 4, and the main conclusions of this work are highlighted in Section 5.

## 2. Background

### 2.1. Relevant EMS Models for Microgrids

This work focuses on centralized controllers for microgrids. If compared with decentralized controllers, these have the advantage of incorporating global knowledge of the system, so that asset management decisions can always be optimal and supply-demand balance can be maintained, which is critical in isolated microgrids. However, the communication and computational burden is higher, since all measurements, setpoints and decisions are integrated in a single controller [25]. The EMS function in microgrids, which may be divided into UC and economic dispatch, is a decision making process which minimizes system operating costs. Two approaches are typical for microgrid EMS design: rules and optimization [26].

EMSs based on logical rules are the most typical and straightforward in microgrids, and follow a decision tree based on system state variables to compute the setpoints of microgrid components. These EMSs can be based on single rules that follow standard combinational or sequential logic (e.g., [27, 28]), or more advanced fuzzy-logic rules (e.g., [29]). They can also follow several rules based on a finite state machine, where the system responds to system inputs that trigger new states with new sets of rules (e.g., [30, 31]).

EMSs based on optimization models minimize an objective function quantifying the operation costs of the microgrid, including fuel costs, start-up and shut-down costs, curtailment costs, and emission costs, among others. This minimization is subject to technical constraints that impose operational limits on the microgrid assets [14, 16, 32]. The main constraint is the power balance, which guarantees that generation and load are equal at all times. Other typical constraints are DG active power limits, start-up and shut-down minimum times, Energy Storage System (ESS) State-of-charge (SoC) computation and limits, and UC variables. In some cases, the EMS model integrates an Optimal Power Flow (OPF) model and a UC model to account for the effect of the distribution grid in the final outcome of the algorithm [32]. In others, a MPC approach is used to tackle the uncertainties of load and renewables by running the EMS model repeatedly in a time scale of minutes, considering the most recent forecast of these variables [16, 32].

### 2.2. Overview of Testing Facility

CANREL is a microgrid testbed located in Guelph, Ontario, Canada, and described in detail in [33], is owned, maintained and operated by Canadian Solar Inc. This microgrid testbed allows the testing of controllers, protection systems, and DGs in real conditions, with a large range of possibilities for load and generation settings. The facility is equipped with two controllable load banks of 100 kW/75 kVar, a diesel genset of 90 kVA, a Li-ion battery of 200 kWh and a maximum output of 200 kVA, a wind energy simulator of 100 kW, a Photovoltaic (PV) simulator

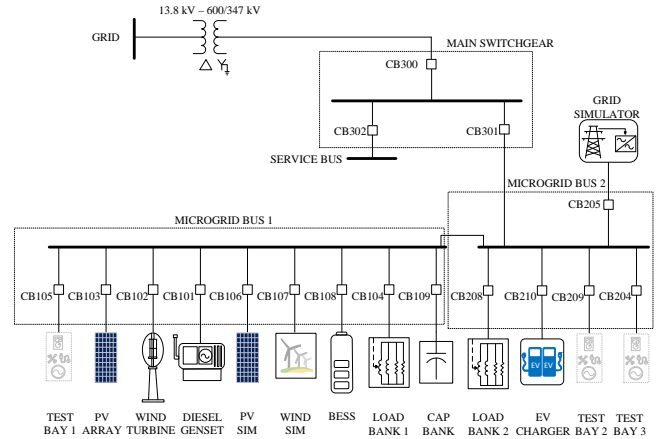


Figure 1: CANREL's architecture.

of 90 kW, a vertical axis wind generator of 3 kW, and a PV array of 10 kW. Moreover, it has an Electric Vehicle (EV) charger for testing the integration of electric transportation into microgrid environments, a grid simulator to test the transition between grid connected and isolated mode operations, a 25 kVar capacitor bank for voltage support, and two connection bays with protection and control devices to test different generation assets in the microgrid. Since the testbed consists of physical power, control, and communication interacting hardware and software components, any issue encountered in these elements may impact the performance of the entire system. Thus, the testbed allows investigating the actual behavior of these components under real phenomena, including communication delays and protocols, computational issues, transient behavior of loads and various generation sources, interaction and operation of control and protection systems, which are not all possible to model in simulation environments such as those used in hardware-in-the-loop studies.

The existing facility was sized to test various possible microgrids that may be found in practice, including a system fully fed by renewable generation with batteries, which is the reason for the large battery compared to other generation systems, as discussed in [33]. Fig. 1 depicts the single-line diagram of the CANREL testbed. Note that the Li-ion battery is the largest capacity source in the CANREL, by design, and that some components, such as the capacitor bank, the EV charger, and the grid simulator, are not used in the EMS tests described in the next sections, since these are not necessary to test, demonstrate, and compare the presented EMS algorithms.

An important aspect of the CANREL testbed is the use of an open communication protocol known as MQTT [34]. This is based on a publish/subscribe pattern that facilitates the integration of equipment from different vendors. The MQTT standard works on TCP/IP protocol and requires a central broker server that receives messages from Asset Controllers, which are communication protocol translators, and re-transmits the message to all agents

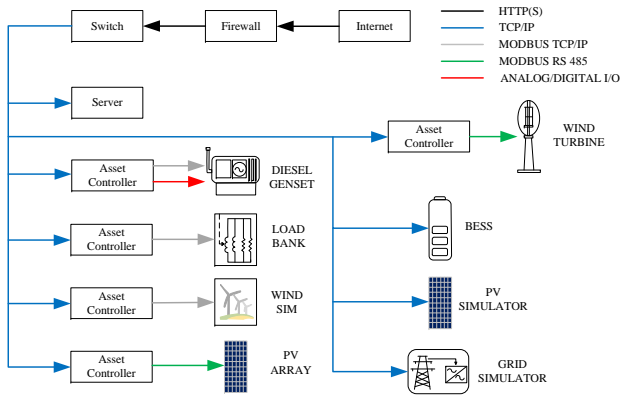


Figure 2: CANREL’s communication network.

that are subscribed to the topics that categorize each message. Each hardware device sends and receives data in a particular protocol to and from an Asset Controller, which converts them to the MQTT protocol and communicates with the broker server through a TCP/IP interface using Ethernet. For example, the diesel genset, the load bank, and the wind simulator connect to the Asset Controller using Modbus on Ethernet, whereas the PV array and wind turbine use Modbus on RS485. In this way, new components can be easily integrated into the microgrid and several types of controllers can be tested using only one protocol, significantly simplifying the development efforts. A general overview of CANREL’s communication network is shown in Fig. 2.

The central broker server of the CANREL implements three types of MQTT message topics. The first category describes the status of each component and is used within the controller to verify the correct operation of the element. The second category is used for measurements from each circuit breaker in the microgrid, listing all electrical variables such as voltage, current, frequency, and active, reactive and apparent power. Finally, the third category implements the control actions of each component to send commands such as active and reactive power setpoints, curtailment levels, lock/unlock signals, and fault resets. Thanks to the aforementioned communication architecture and the available message topics, a simple desktop, with an Ethernet connection and the required permissions to access the CANREL’s network and communicate with the broker server, can be used to implement and test EMS algorithms in the testbed. The EMS implementations are described next, and are independent of the chosen programming language, as long as it supports the MQTT protocol.

### 3. EMS Algorithms

This section details two EMS algorithms which were implemented in the CANREL. As the CANREL contains only one physical diesel genset, a second diesel genset has

been modelled in the EMS algorithm, and the calculated setpoints for the second diesel genset have been combined with the wind and solar generation curves to control the simulators during testing, as discussed in the next subsections. The main purpose of this approach is to increase the availability of dispatchable, non-renewable sources, and compare the performance of DG units with different cost functions.

#### 3.1. Rule-based EMS (RBEMS)

A RBEMS based on a state machine is used to dispatch the units of the CANREL testbed, as depicted in Fig. 3. This algorithm contains six different states, according to the commitment of the two assumed diesel genset units, and the curtailment of renewable generation or load resources, depending on the operation conditions of the battery, which is the main source in this system. The following are the states of the algorithm depicted in Fig. 3, based on trying to minimize the use of the diesel genset:

- *State 1—Battery Only*: This is the normal state of the microgrid given the size of the battery, and its low operating costs, being called immediately after starting the EMS. In this state, the battery is used as the main source to balance supply and demand. This state can either transition to States 2, 3 or 5, according to the battery SoC. When the battery SoC is low, the transition is made to States 2 and 3, which commit Diesels 1 and 2, respectively. The order of commitment between diesel gensets is defined by the cost of the energy output required at the moment at which the SoC reaches the minimum limit. This energy is calculated so that it covers the load and a constant amount of power to recover the battery SoC, which in this case is assumed to be the minimum output of the diesel gensets. In contrast, the transition to State 5 is achieved when the battery SoC reaches a maximum limit, as explained below.
- *State 2—Diesel 1*, and *State 3—Diesel 2*: These states are used respectively to commit Diesels 1 and 2, following a low battery SoC, since the microgrid requires more resources to maintain the power balance.<sup>1</sup> The transition from States 2 or 3 can be either to State 4, or back to State 1. The change to State 4 is achieved when the load cannot be fulfilled completely by the committed diesel genset, or when the reserve cannot be fulfilled entirely by the committed unit. In general, the reserves are assumed to be 10% of the load, 25% of the PV generation, and 50% of the wind generation, as per [35]. The transition to State 1 happens when the battery SoC reaches 20%

<sup>1</sup>In the case of Diesel 1, the output at which the unit is committed is *held constant* until the unit is turned off. This requirement is non-standard, and is due to the particularities of Diesel 1 in CANREL, which only responds to an initial PQ command when it is committed.

more than the minimum level and the diesel units have operated for a longer time than their minimum runtime, so that the battery has at least a minimum amount of energy to keep the system running without the diesel genset units. In this case, the turn off signals of the corresponding diesel units are activated to signal the transition to State 1.

- *State 4—Diesel 1 and 2:* In this state, both the Diesels 1 and 2 are committed to fulfill the load demand and keep the reserve limits without the participation of the battery. The main goal here is to produce enough energy to feed the load and charge the battery. When the system is operating in State 4, it can transition back to States 2 or 3, or to State 6, which represents load curtailment. The transition to States 2 or 3 is done when the SoC has reached a level 20% above the minimum limit, and the units have run for a minimum time; the order between States 2 or 3 is defined in terms of the unit that has run for a longer time, since this is decommitted first. The transition to State 6 occurs when the two diesel gensets are not able to supply completely the load demand.
- *State 5—Renewable Generation Curtailment:* This state is activated when the available generation of the PV or the wind cannot be stored in the battery, since its SoC has reached a maximum limit. In this state, both renewables are turned off to accelerate the discharging of the battery. It transitions back to State 1 when the battery is discharged to a level 20% below the maximum limit. It is important to mention that in actual isolated microgrids with relatively small-sized renewable energy sources, as in the case of CANREL, these sources are typically turned off to curtail their output, as these units usually do not have power control capabilities, operating only in Maximum Power Point Tracking (MPPT) control mode.
- *State 6—Load Curtailment:* This state is called when the battery is depleted and generation resources are not enough to supply the load. Thus, the load is limited to a level below the available generation resources, and is kept in that state until the battery reaches a level 20% higher than the minimum limit, at which point the system goes back to State 4.

Each state has a polling action that is called every  $T$  seconds (normally 300s), to update the values of the input variables and trigger the evaluation of the set of rules of the current state, and the possible transition to a new state.

### 3.2. Optimization-based EMS (OBEMS)

The OBEMS implements a UC model for this particular microgrid, based on the model proposed in [32], as follows:

- *Objective Function:* The objective is the minimization of generation costs over a future time horizon, following a linear function which is calculated from the heat rate of the diesel genset units. The start-up and shut-down costs of the diesel units are also incorporated, along with the costs incurred due to any required curtailment of renewable generation resources and loads. Mathematically, the minimization problem of interest is:

$$\text{minimize } \sum_{k_t \in \mathcal{T}_t} \sum_{d \in \mathcal{D}} J_{d,k_t}^{gen} + \sum_{k_t \in \mathcal{T}_t} J_{k_t}^{cur} \quad (1)$$

where

$$J_{d,k_t}^{gen} = (a_d^g P_{d,k_t} + b_d^g) \Delta t_{k_t} + C_d^{sup} U_{d,k_t} + C_d^{sdn} V_{d,k_t}$$

$$J_{k_t}^{cur} = (C_{pvs}^{cur} P_{pvs,k_t}^{cur} + C_{ws}^{cur} P_{ws,k_t}^{cur} + C_{lb}^{cur} P_{lb,k_t}^{cur}) \Delta t_{k_t}$$

All variables and parameters in this and other equations are defined in the Nomenclature section at the beginning of the paper. The next constraints are enforced at all prediction times  $k_t \in \mathcal{T}_t$ .

- *Load Balance:* The following equation guarantees that the load is properly supplied:

$$P_{d1,k_t} + P_{d2,k_t} + P_{b,k_t} + P_{ws,k_t} + P_{pvs,k_t} - P_{ws,k_t}^{cur} - P_{pvs,k_t}^{cur} = P_{lb,k_t} - P_{lb,k_t}^{cur}. \quad (3)$$

- *Dispatchable Generation Output Limits:* These constraints represent the limits of the diesel generators and battery:

$$\underline{P}_d W_{d,k_t} \leq P_{d,k_t} \leq \overline{P}_d W_{d,k_t}, \quad d \in \mathcal{D}, \quad (4a)$$

$$\underline{P}_b W_{b,k_t} \leq P_{b,k_t} \leq \overline{P}_b W_{b,k_t}. \quad (4b)$$

- *Battery Active Power Decomposition:* The following equations first decompose the battery active power signal into two positive components for charging and discharging, and then guarantee that these two variables are complementary:

$$P_{b,k_t} = P_{b,k_t}^{out} - P_{b,k_t}^{in}, \quad (5a)$$

$$P_{b,k_t}^{in} \perp P_{b,k_t}^{out}. \quad (5b)$$

- *Diesel 1 Constraints:* The following equations are different from the typical unit commitment formulation, since they correspond to a particular condition of the diesel genset in the CANREL microgrid testbed:

$$P_{d1,k_t} = K D_{d1,k_t} \overline{P}_{d1} \quad (6a)$$

$$W_{d1,k_t} \underline{K} D_{d1} \leq K D_{d1,k_t} \leq W_{d1,k_t} \overline{K} D_{d1} \quad (6b)$$

$$K D_{d1,k_t} \geq K D_{d1,k_t-1} - V_{d1,k_t} \overline{K} D_{d1} \quad (6c)$$

$$K D_{d1,k_t} \leq K D_{d1,k_t-1} + U_{d1,k_t} \overline{K} D_{d1}. \quad (6d)$$

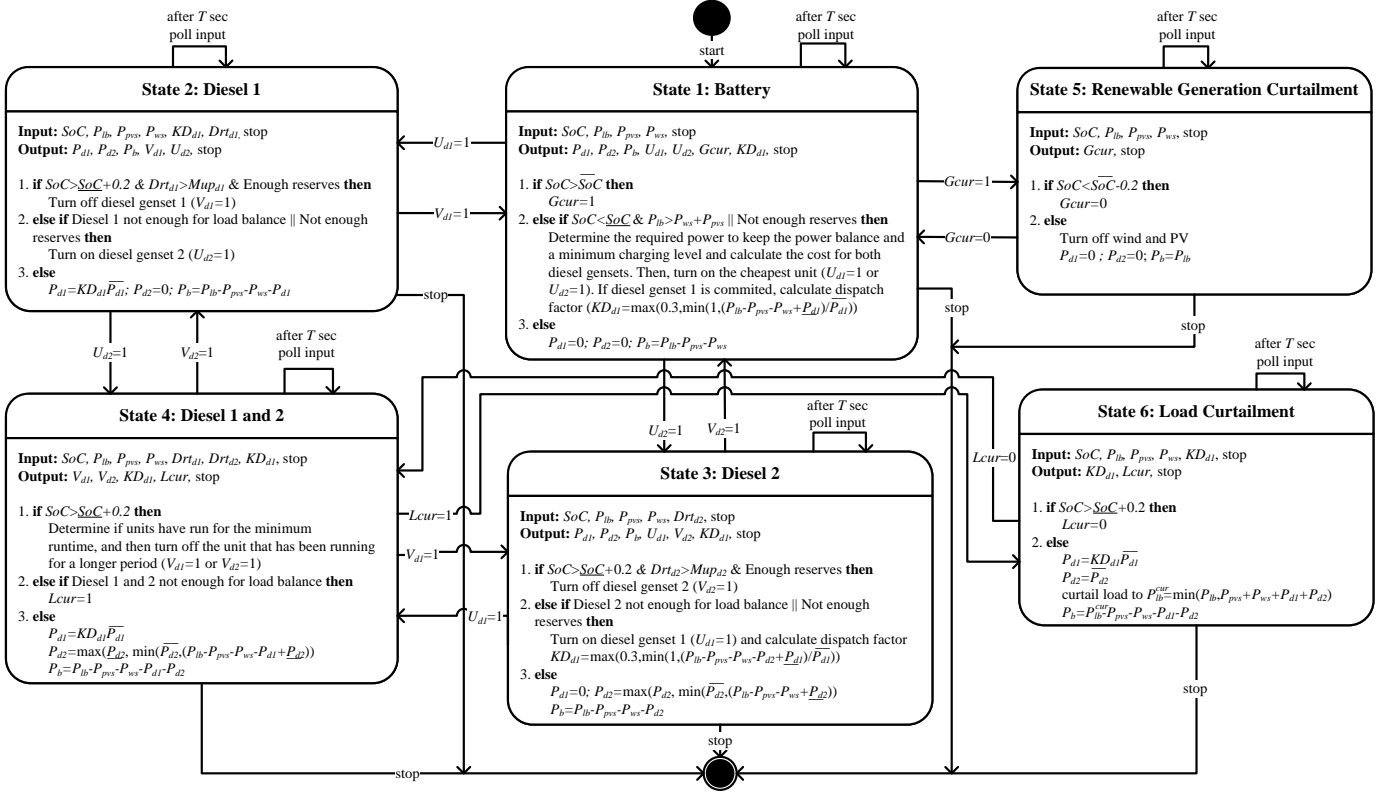


Figure 3: State diagram of the RBEMS.

Since the diesel genset output cannot be changed during the commitment period, this set of constraints is used to recalculate the active power output each time the generator is committed.

- **Battery SoC Constraints:** These equations represent the SoC of the battery and its limits:

$$SoC_{b,k_t+1} = SoC_{b,k_t} + \left( P_{b,k_t}^{in} \eta_b^{in} - \frac{P_{b,k_t}^{out}}{\eta_b^{out}} \right) \Delta t_{k_t}, \quad (7a)$$

$$\underline{SoC}_b \leq SoC_{b,k_t} \leq \overline{SoC}_b. \quad (7b)$$

- **Constraints for UC Variables:** The following equations assure the correct sequence of turn-on and turn-off signals for dispatchable diesel units in the micro-grid:

$$U_{d,k_t} - V_{d,k_t} = W_{d,k_t} - W_{d,k_t-1}, \quad d \in \mathcal{D}, \quad (8a)$$

$$U_{d,k_t} + V_{d,k_t} \leq 1, \quad d \in \mathcal{D}. \quad (8b)$$

- **Minimum Up-time and Down-time Constraints:** The following equations describe the minimum times that diesel units should be turned on or off before chang-

ing to a new state:

$$\sum_{\hat{k}_t: t_{\hat{k}_t} = t_{k_t} - M_{up,d}}^{k_t-1} W_{d,\hat{k}_t} \Delta t_{\hat{k}_t} - M_{up,d} V_{d,k_t} \geq 0 \quad (9a)$$

$$M_{dn,d}(1 - U_{d,k_t}) - \sum_{\hat{k}_t: t_{\hat{k}_t} = t_{k_t} - M_{dn,d}}^{k_t-1} W_{d,\hat{k}_t} \Delta t_{\hat{k}_t} \geq 0 \quad (9b)$$

- **Ramp-up and Ramp-down Constraints:** The following equations represent the diesel unit ramping limits follow when they go from zero to full load, and from full to zero:

$$P_{d,k_t+1} - P_{d,k_t} - U_{d,k_t+1} \overline{P}_d \leq R_{up,d} \Delta t_{k_t} \quad (10a)$$

$$P_{d,k_t} - P_{d,k_t+1} - V_{d,k_t+1} \overline{P}_d \leq R_{dn,d} \Delta t_{k_t} \quad (10b)$$

- **Load and Generation Curtailment:** The following equations define the curtailment levels for the wind and PV simulators and the load bank:

$$P_{ws,k_t}^{cur} = W_{ws,k_t}^{cur} P_{ws,k_t} \quad (11a)$$

$$P_{pvs,k_t}^{cur} = W_{pvs,k_t}^{cur} P_{pvs,k_t} \quad (11b)$$

$$0 \leq P_{lb,k_t}^{cur} \leq P_{lb,k_t}. \quad (11c)$$

Note that the curtailment power from the PV and wind simulators correspond to the total available power, as these operate in MPPT mode, which means that these simulators are turned off when the curtailment signal  $W^{cur} = 1$ .

- *Minimum Spinning Reserve*: The following equations describe the minimum generation capacity that should be committed to compensate for the variations in generation and load:

$$\sum_{d \in \mathcal{D}} W_{d,k_t} [\bar{P}_d - P_{d,k_t}] + W_{b,k_t} [\bar{P}_b - P_{b,k_t}] \geq \quad (12)$$

$$R_{s_{pvs}} P_{pvs,k_t} + R_{s_{ws}} P_{ws,k_t} + R_{s_{lb}} P_{lb,k_t}$$

As proposed in [32], the MPC method is used here to tackle the uncertainties of renewables and loads. The optimization model is solved every 5 minutes with the most recent forecasts for renewables and loads, and updated measurements from the microgrid, but only the setpoints calculated for the first time step are actually sent to the dispatchable generators. To improve the solution speed of the optimization model, a variable time step is considered for the 24-hour look-ahead window, where  $\mathcal{T}_t$  indexes the prediction times forward from time  $t$ . Thus, the 30 minutes is divided in six steps of 5 min, the next 90 minutes is divided in six steps of 15 min, the following 3 hours are divided in six steps of 30 min, and the last 19 hours are divided into 19 one-hour time steps.

### 3.3. EMSs Implementation at CANREL

The EMSs explained in the previous subsection were implemented in the CANREL testbed to perform several tests with various load and generation conditions. For this purpose, an application in Python language was developed, integrating several commands for control and visualization. Since one of the main features of this application was the use of open-source software, the package Pyomo for optimization problem modeling [36], and the COIN-OR branch and cut (CBC) solver in [37] were used in this implementation. The GLPK solver is another possible free option to implement the EMS, but the CBC solver was selected as it performs better for Mixed-integer Linear Programming (MILP) problems [38]. To establish the communication between the application and the microgrid broker server, the Paho client library for Python in [39] was used to implement an MQTT client to translate all the setpoints calculated with the EMS algorithms into the corresponding topics available in the microgrid, and to read all measurements of generation and load assets.

A Graphical User Interface (GUI) was implemented to ease the operation of the application. This GUI was coded using PyQt library in Python [40], deploying the measurements of the microgrid assets and allowing the user to run independently different components of the microgrid. The interface was divided into three parts: manual mode, RBEMS, and OBEMS. In manual mode, each component

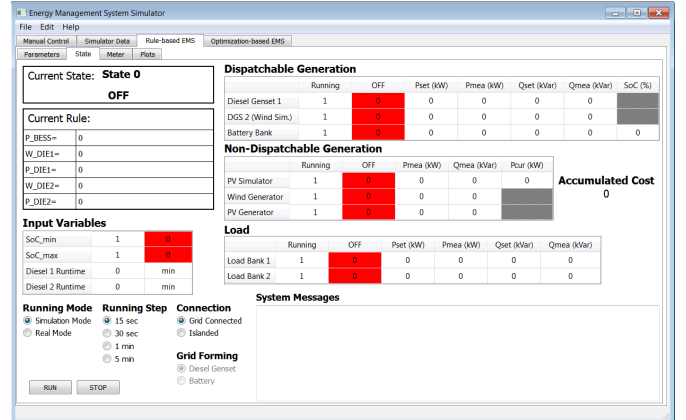


Figure 4: Rule-based EMS tab.

of the microgrid can be controlled independently using all the available MQTT topics in the system. The purpose of this mode is primarily diagnostic, to check that all messages are received correctly by the broker server, and that the microgrid measurements are appropriately received.

The RBEMS mode includes four tabs. The first tab allows the user to input the technical and cost parameters of the diesel gensets and the battery. The second tab contains toggle buttons to select the type of simulation and the intervals for calculating new setpoints, as well as displaying tables to show the current state of the system, the last setpoints, and the last measurements. The third tab includes all measurements and energy calculations of the microgrid components, and the fourth tab shows the time plots comparing the setpoints and actual measurements of generation and loads. In the case of the OBEMS, the tab has a very similar structure compared to the RBEMS, with the main difference of an additional tab in the OBEMS that shows the output of the solver in each iteration of the MPC. An overview of the main RBEMS tab is presented in Fig. 4.

## 4. Test Results and Discussion

In order to test the performance of the two EMS algorithms previously discussed, two cases with different load and generation conditions were designed, following the renewable and load curves depicted in Fig. 5 extracted from [41]. The diesel genset unit of CANREL is a 90 kW DS-GAA model with engine QSB7 from Cummins, and thus, the heat rate data was taken from the corresponding specification sheet [42]. With this information, and taking an average diesel price for Ontario for April 15 of 2019 of 1.23 CAD/L [43], the heat rate of the diesel genset was approximated to a linear function equal to  $(0.34P_{d1} + 7.08)\Delta t_{k_t}$ . For the second simulated diesel genset, the cost function was assumed as  $(0.42P_{d2} + 3.26)\Delta t_{k_t}$ , which, compared to Diesel 1, gives a cheaper cost when the output is less than 60 kW, and a more expensive value otherwise. The start-up costs for both diesel gensets were assumed

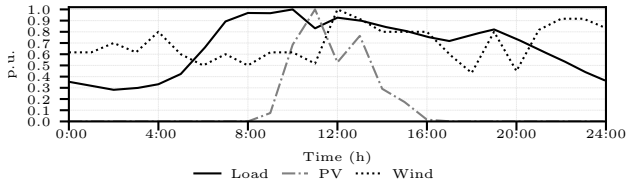


Figure 5: Load and generation curves for testbed elements.

to be 5 CAD and 7.5 CAD, and the shut down costs were assumed to be 1.5 CAD and 2 CAD, respectively.

In the first test case (Case 1), the load is given a base value of 60 kW, and the PV and wind curves are assigned a base value of 25 kW. In the second test case (Case 2), the base value for the load, PV, and wind generation is 50 kW. Note that the load and generation values do not follow an optimal sizing procedure, with the load peak value in Case 1 being chosen to be more than twice the individual values of each renewable source, while in Case 2 the load and renewables peak values are equal, so that two significantly different cases can be studied.

The MPC in the OBEMS assumes perfect forecasts, based on the load and solar and wind generation curves of Fig. 5, with the latter being integrated into the Wind Simulator, together with a Diesel 2 model. As demonstrated in [44], assuming a perfect forecast in an MPC-based microgrid EMS will give the lowest cost result, from which the effect of forecasting uncertainties can be studied, although this is not the goal of this paper. Moreover, the minimum and maximum SoC battery limits are set, without loss of generality, to 25% and 90%, and the initial SoC is assumed to be 50%.

The two aforementioned cases for both EMS algorithms are first run in simulation mode and discussed in Section 4.1, to analyze the dispatch response, without sending the set points to testbed elements. Then, the real testbed measurements for two of the proposed experiments are presented in Section 4.2.

#### 4.1. Simulations

The dispatch results for Case 1 are presented in Fig. 6. Note that the RBEMS commits Diesel 1 alone (State 2) three times, Diesel 2 alone (State 3) once, and both Diesels 1 and 2 (State 4) once. In contrast, the OBEMS commits Diesel 1 alone twice, Diesel 2 alone twice, and does not commit simultaneously Diesels 1 and 2. Thus, the start-up and shut-down costs of the OBEMS are lower than the costs of the RBEMS, as shown in Table 1. However, the total delivered energy and thus, the total energy costs are higher in the OBEMS, since the battery stores more energy at the end of the period, as seen in the final value of battery SoC in Table 1 and Fig. 6 (c). The extra energy that is stored in the battery is explained by the look-ahead window of the MPC approach implemented in the OBEMS, since the forecasted load and renewable generation conditions for the next day, which are assumed to

Table 1: Total costs and energy consumption for different tests.

	Case 1		Case 2	
	RBEMS	OBEMS	RBEMS	OBEMS
Total delivered energy [kWh]	980.89	1047.36	917.41	853.76
Total diesel energy [kWh]	478.12	544.59	0	0
Final SoC [%]	28.43	63.54	80.55	46.89
Total curtailed generation [kWh]	0	0	88.13	151.78
Total diesel energy cost [CAD]	219.58	240.89	-	-
Total start-up and shut-down costs [CAD]	45	32	-	-
Total diesel cost [CAD]	264.58	272.89	-	-
Total diesel cost/kWh [CAD/kWh]	0.55	0.50	-	-

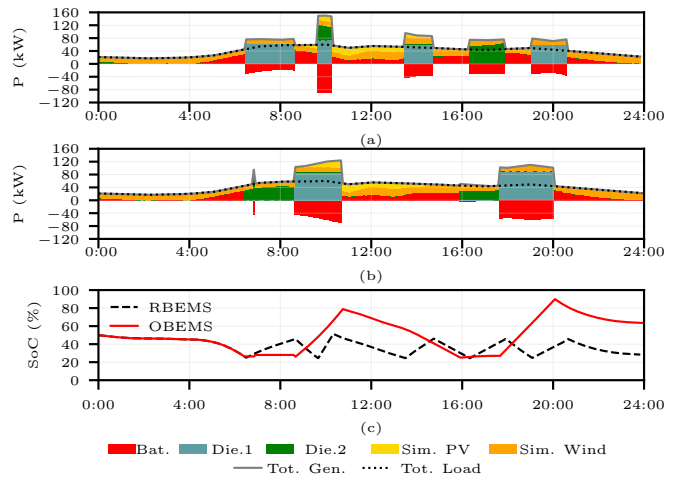


Figure 6: Dispatch results for Case 1: (a) RBEMS, (b) OBEMS, and (c) Battery SoC.

be the same, will require this energy to achieve cost reductions. Thus, to give a comparable framework between both algorithms and account for the difference in delivered energy, the cost per kWh is calculated for all cases and algorithms, as shown in the last row of Table 1. Note that, for Case 1, the OBEMS gives a lower unitary value of energy compared to the RBEMS, as expected.

The results for Case 2 are presented in Fig. 7. In both scenarios the diesel gensets are never committed, as the renewable generation and the battery are enough to supply the load demand. The RBEMS curtails the renewable generation twice during the day, since the battery SoC reaches the maximum limit and the surplus energy cannot be appropriately stored. The OBEMS curtails more energy than the RBEMS, as illustrated in Table 1, due to the effect of the look-ahead window in this approach. As seen in Fig. 7(b), the OBEMS starts curtailing renewables at the beginning of the day, whereas the RBEMS only does it around noon, when the SoC of the battery reaches the maximum limit. Note that, just after 12:00, PV and wind are curtailed and the battery is discharged in the OBEMS case, even though the renewable generation is sufficient to supply the load demand. This is due to the existing PV and wind systems only accepting on/off commands, i.e.,

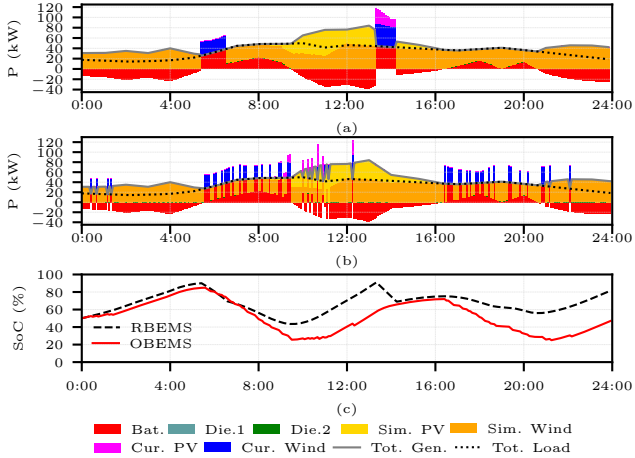


Figure 7: Dispatch results for Case 2: (a) RBEMS, (b) OBEMS, and (c) Battery SoC.

they cannot be operated at reduced power. Furthermore, the dispatch decisions are not only taken based on the current system conditions, but also based future conditions via the MPC approach. Current set-points therefore take into consideration the load, generation, and storage constraints at future times. At the end of the day, the OBEMS keeps the battery SoC closer to the initial value, whereas the RBEMS reaches a value that is close to the maximum limit. Because of this, the curtailment on the RBEMS will be higher than the OBEMS in the next operating day.

#### 4.2. Testbed Measurements

The actual measurements on CANREL for the RBEMS algorithm in Case 1 are presented in Fig. 8. The aforementioned setpoints produced by the EMS algorithm were sent to the CANREL assets every 15 s, instead of 5 min, to speed up the simulation for the 24 h curve; thus, a full simulation of 288 points was completed in 72 min, as reflected in the two time axis. Fig. 8(a) depicts the response of the load bank, which is composed of switchable resistance banks of 5 kW per step, explaining the mismatch between the setpoint and the actual measurement. Fig. 8(b) presents the results for Diesel 1, where the unit is committed four times, with the power levels remaining constant when the unit is committed, as explained previously in Sect. 3.2; these are always higher than 60 kW, as the cost function makes this unit cheaper at this output level. Moreover, observe a delay between the setpoint and the actual measurement, which is more noticeable the second time the unit is committed, and can be attributed to the communication system and the diesel genset controller. The battery response is seen in Fig. 8(c), which presents a very good match between the setpoint and the actual measurement.

Fig. 8(d) shows the response of the Wind Simulator, which follows the sum of three setpoints: Diesel 2, and simulated PV and wind power, as previously mentioned.

The actual response of the wind simulator is very close to the setpoint, as expected, with a slightly higher mismatch compared to the battery.

Fig.8(e) presents the measurements of the PV array and the wind turbine. Note that the total output of the PV array does not surpass 2 kW or 20% of the peak capacity, since this test was carried out during a cloudy day. Moreover, the wind turbine output is always negative, which represents the losses of the connection transformer, as the wind speed during the period of the test in the microgrid location was very low.

Finally, the measurements at the grid connection point are presented in Fig. 8(f), since the tests were performed in grid-connected mode because of control and protection system's constraints on the testbed, which do not allow it to operate in isolated mode, and also because the main focus of the paper is the implementation and analysis of different EMSs, rather than the study of the operation and response of the microgrid and its components in different connection modes, as discussed in [33]. This curve represents the mismatch between generation and load, due to the EMS time intervals and the differences and delays between the setpoints and the actual measurements of different microgrid components. If the same test is carried out in isolated mode, all these differences would have been compensated by the primary controllers of the battery and/or Diesel 1 to maintain the system frequency and voltage.

The testbed results for the OBEMS algorithm in Case 2 are depicted in Fig. 9, under the same aforementioned testing conditions for Case 1 RBEMS. The setpoints and the measurements in this case are also close together, even though the setpoints for the battery and the wind simulator vary more often because of the curtailment commands calculated by the OBEMS. Moreover, solar conditions were better during this test, as the PV array output, presented in Fig. 9(e), reached values above 8 kW for a large portion of the simulation run. A noticeable delay occurred at some points during the simulation, due to the optimization solver taking longer than the 15 s running window that was set up for the simulation. This particular condition was seen when the load curve was increasing between 6 am and 10 am, with the MPC runs for some points in this interval taking between 40 s and 5.5 min to be solved, which would not be a significant problem in a real application, since the solution intervals would be 5 min or longer. We observe that there are 15 charge/discharge and 15 discharge/charge transitions over 288 setpoints. As the battery current is always below 1C, these changes do not degrade the battery. If desired however, additional constraints to limit the number of battery operations could be added to both EMS formulations to reduce possible battery degradation.

Due to existing hardware and software within the CANREL, actuation and communication delays were found to be significant. Two boxplots are used here to represent the measured response delays of different testbed components, and are presented in Figs. 10 and 11. These delays are

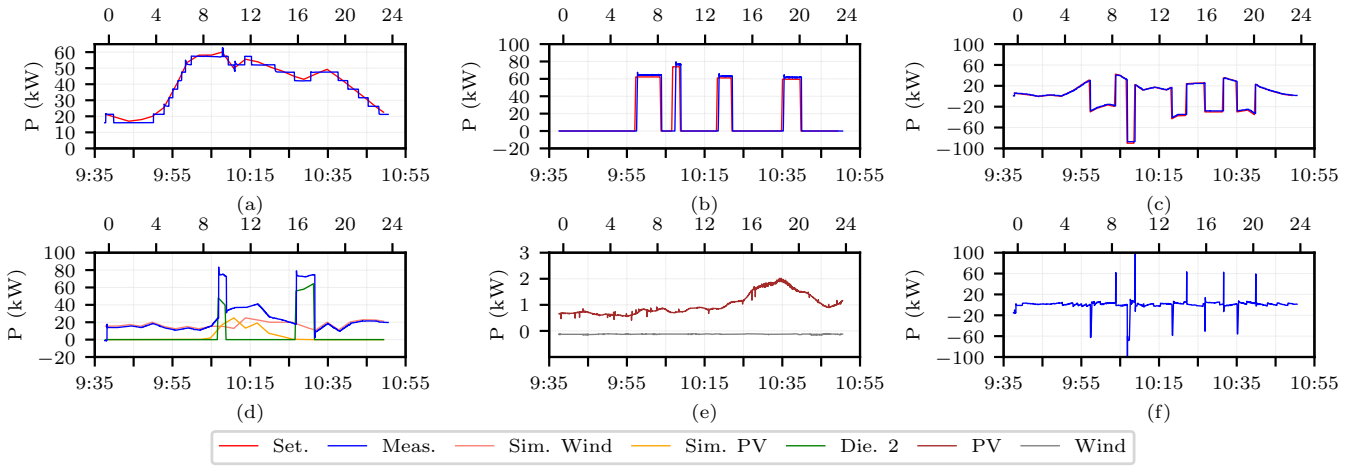


Figure 8: Response of different testbed elements for Case 1 RBEMS: (a) load bank, (b) diesel genset, (c) battery bank, (d) wind simulator, (e) PV array and wind turbine, and (f) grid connection point.

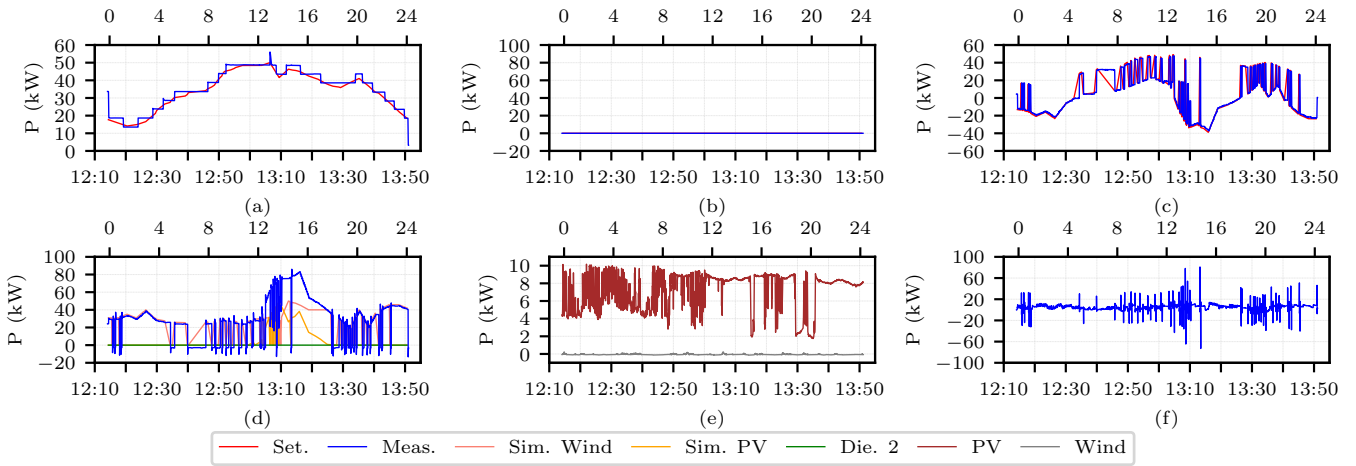


Figure 9: Response of different testbed elements for Case 2 OBEMS : (a) load bank, (b) diesel genset, (c) battery bank, (d) wind simulator, (e) PV array and wind turbine, and (f) grid connection point.

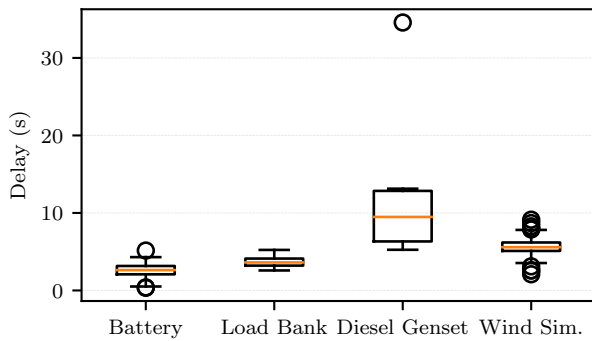


Figure 10: Response delays of different testbed elements for Case 1 RBEMS.

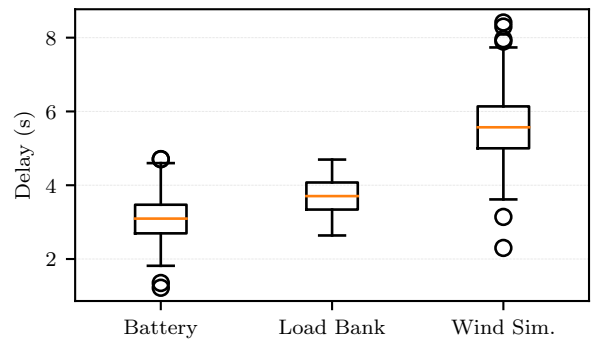


Figure 11: Response delays of different testbed elements for Case 2 OBEMS.

computed as the difference between the setpoint timestamp and the corresponding response timestamp, mea-

sured on the device circuit breaker (e.g., the response delay of the battery bank was measured at CB108). These

delays also represent the performance of the communication link, the MQTT protocol, and the device controller in response to dispatch setpoints. Observe in Fig. 10 that the response delay medians of different testbed elements in Case 1 RBEMS are: 2.63 s for the battery bank, 3.61 s for the load bank, 9.48 s for the diesel genset, and 5.58 s for the wind simulator. On the other hand, for Case 2 OBEMS in Fig. 11, the response delay medians are: 3.09 s for the battery bank, 3.70 s for the load bank, and 5.57 s for the wind simulator. The median response delays in both test cases are very similar and expected; in particular, the diesel genset — whose delays are only computed in Case 1 RBEMS, as it is not dispatched in Case 2 OBEMS — has a median response delay of 9.48 s, which is consistent with the response time of 10 s that is expected for this generator model [42]. However, observe in Fig. 10 that the diesel genset response delay presents an outlier of 34.57 s, which is far from the median and is associated with the first turn-on command after being inactive, thus taking longer to warm up and inject active power to the microgrid.

In terms of computation times, from 288 optimization points calculated in Case 2 OBEMS, 2 of optimization points took more than 100 s (the maximum computation time was 318.15 s), 32 points took between 10 s and 100 s, 48 points took between 10 s and 1 s, and the remaining 206 points took less than 1 s. These times are acceptable, and are consistent with the considered 5 min interval windows used in the OBEMS. For Case 1 RBEMS, only 6 out of 288 dispatch points took between 1 s and 10 s (the maximum was 7.33 s), while the remaining 282 points took less than 1 s, which is to be expected given the simplicity of the calculations inside the RBEMS.

#### 4.3. Discussion

The computational requirements of the RBEMS are lower than the OBEMS, as the former follows simple sequential logic rules, whereas the latter uses optimization solvers that may require significant computational resources as the number of variables and the size of the look-ahead window increases. The performance of the RBEMS depends largely on translating the microgrid operation experience into an appropriate sets of rules; this can be time consuming, as the operator must identify in practice the typical and emergency conditions of the microgrid. In contrast, the performance of the OBEMS depends largely on the tools available for solving the optimization problem and accurate forecasts, even though some operator experience is also required for tuning the technical parameters of the optimization model. If the OBEMS receives reasonable forecasts and the optimization problem can be solved reliably, it can reduce the operating costs more easily than the RBEMS, and can also integrate other technical and environmental constraints, such as battery degradation and emissions. Thus, for practical EMS applications, both algorithms can be combined in such a way that the RBEMS takes control of the microgrid when the OBEMS is not able

to find a solution in a specified solution window, as was experienced during the Case 2 OBEMS testing. To implement this approach, the optimization solution time in the OBEMS should be continually monitored and compared to a maximum limit so that, when this limit is surpassed, the RBEMS solves the current dispatch point considering the latest microgrid conditions.

The MQTT standard in the testbed showed a good performance in terms of latency. It usually took less than 1 s from the moment the setpoints were generated to the instant a response message produced by the broker server was received, which is fast enough for correct EMS operation. Moreover, the subscribe/publish pattern of this protocol facilitates the EMS development and implementation, as well as the integration of new hardware into the microgrid, since the topics for control and measurements can be reproduced and adapted without much effort. However, MQTT relies on a client/server topology for message distribution, which compared to other protocols used in smart grid applications, such as those included in the standard IEC 61850, may not be suitable for fast microgrid control and protection [45].

From this study, some considerations for microgrid development and implementation can be identified in terms of facilitating the integration of an EMS system. Thus, apart from the optimal selection and sizing of generation and storage resources, it is important to clearly define the measurement, communication, and computation requirements. As a first step, the electrical variables to be measured, the frequency of measurement, and the correct location of measuring devices should be properly identified, as these vary according to the EMS algorithm to be implemented. Then, a communication protocol that facilitates the integration of control and measuring devices from different vendors, and has a good response time for EMS, should be selected; in this study, the MQTT standard, which was primarily designed for IoT applications, showed a good performance. Finally, the hardware required to process the measurement signals, solve the EMS algorithms, and send the set points to the microgrid's components in a convenient time should be carefully selected, considering that algorithms such as the OBEMS require more computational resources to guarantee correct microgrid operation.

## 5. Conclusion

This paper presented the implementation and testing of two EMS algorithms on the CANREL microgrid testbed. The first algorithm comprised several rules that were designed to maintain the normal balance of load and generation with the help of a battery bank, while reducing the utilization of diesel gensets, whereas the second algorithm followed a UC model that minimized the total operation costs of the microgrid. Both algorithms were coded in Python, using different open-source libraries for GUI design, optimization, and communication. The tests on the

CANREL showed a better performance of the OBEMS in terms of unitary energy costs, exhibiting typical issues in microgrid operation, such as communication delays and mismatches between the setpoints and real measurements, which are common in real implementations and should be considered in EMS controller design. Future work includes the improvement of the EMS tests by including uncertainty in renewables emulation, and the effect of primary controllers in isolated mode operation.

## Acknowledgement

This work was supported by the National Sciences and Engineering Research Council (NSERC) of Canada and Canadian Solar Inc.

## References

- [1] D. Stenclik, P. Denholm, and B. Chalamala, "Maintaining balance: The increasing role of energy storage for renewable integration," *IEEE Power Energy Mag.*, vol. 15, no. 6, pp. 31–39, 2017.
- [2] A. Ali, W. Li, R. Hussain, X. He, B. W. Williams, and A. H. Memon, "Overview of current microgrid policies, incentives and barriers in the European Union, United States and China," *Sustainability*, vol. 9, no. 7, p. 1146, 2017.
- [3] Navigant Research, "Microgrid Deployment Tracker 4Q18." [Online]. Available: <https://www.navigantresearch.com/reports/microgrid-deployment-tracker-4q18>
- [4] A. Vijay, S. Doolla, and M. C. Chandorkar, "Real-time testing approaches for microgrids," *IEEE J. Emerg. Sel. Topics Power Electron.*, vol. 5, no. 3, pp. 1356–1376, 2017.
- [5] F. Baccino, A. Brissette, D. Ishchenko, A. Kondabathini, and P. Serra, "Real-time hardware-in-the-loop modeling for microgrid applications," in *IEEE 6th International Conference on Clean Electrical Power (ICCEP)*, 2017, pp. 152–157.
- [6] C. M. Rangel, D. Mascarella, and G. Joos, "Real-time implementation & evaluation of grid-connected microgrid energy management systems," in *IEEE Electrical Power and Energy Conference (EPEC)*, 2016, pp. 1–6.
- [7] G. Casolino, M. Russo, P. Varilone, and D. Pescosolido, "Hardware-in-the-loop validation of energy management systems for microgrids: A short overview and a case study," *Energies*, vol. 11, no. 11, p. 2978, 2018.
- [8] M. C. Magro, M. Giannettoni, P. Pinceti, and M. Vanti, "Real time simulator for microgrids," *Electric Power Systems Research*, vol. 160, pp. 381–396, 2018.
- [9] B. Xiao, M. Starke, G. Liu, B. Ollis, P. Irminger, A. Dimitrovski *et al.*, "Development of hardware-in-the-loop microgrid testbed," in *IEEE Energy Conversion Congress and Exposition (ECCE)*, 2015, pp. 1196–1202.
- [10] M. O. Faruque, T. Strasser, G. Lauss, V. Jalili-Marandi, P. Forsyth, C. Dufour, V. Dinavahi, A. Monti, P. Kotsampopoulos, J. A. Martinez *et al.*, "Real-time simulation technologies for power systems design, testing, and analysis," *IEEE Power Energy Technol. Syst. J.*, vol. 2, no. 2, pp. 63–73, 2015.
- [11] E. Hossain, E. Kabalci, R. Bayindir, and R. Perez, "Microgrid testbeds around the world: State of art," *Energy Conversion and Management*, vol. 86, pp. 132–153, 2014.
- [12] N. Lidula and A. Rajapakse, "Microgrids research: A review of experimental microgrids and test systems," *Renewable and Sustainable Energy Reviews*, vol. 15, no. 1, pp. 186–202, 2011.
- [13] M. Marzband, A. Sumper, A. Ruiz-Álvarez, J. L. Domínguez-García, and B. Tomoiagă, "Experimental evaluation of a real time energy management system for stand-alone microgrids in day-ahead markets," *Applied Energy*, vol. 106, pp. 365–376, 2013.
- [14] M. Marzband, A. Sumper, J. L. Domínguez-García, and R. Gumara-Ferret, "Experimental validation of a real time energy management system for microgrids in islanded mode using a local day-ahead electricity market and minlp," *Energy Conversion and Management*, vol. 76, pp. 314–322, 2013.
- [15] Z.-r. Xu, P. Yang, Z. Chen, C.-m. Yang, Q.-r. Zheng, and C.-l. Zheng, "Energy management strategy for medium-voltage isolated microgrid," in *IEEE Industrial Electronics Society Conference (IECON)*, 2015, pp. 80–85.
- [16] A. Parisio, E. Rikos, G. Tzamalís, and L. Glielmo, "Use of model predictive control for experimental microgrid optimization," *Applied Energy*, vol. 115, pp. 37–46, 2014.
- [17] F. Delfino, G. Ferro, M. Robba, and M. Rossi, "An energy management platform for the optimal control of active and reactive powers in sustainable microgrids," *IEEE Trans. Ind. Appl.*, vol. 55, no. 6, pp. 7146–7156, 2019.
- [18] W. C. Clarke, M. J. Brear, and C. Manzie, "Control of an isolated microgrid using hierarchical economic model predictive control," *Applied Energy*, vol. 280, p. 115960, 2020.
- [19] C. Sobin, "A survey on architecture, protocols and challenges in IoT," *Wireless Personal Communications*, vol. 112, pp. 1183–1429, 2020.
- [20] M. Moghimi, J. Liu, P. Jamborsalamati, F. H. M. Rafi, S. Rahman, J. Hossain *et al.*, "Internet of things platform for energy management in multi-microgrid system to improve neutral current compensation," *Energies*, vol. 11, no. 11, p. 3102, 2018.
- [21] M. Moghimi, P. Jamborsalamati, J. Hossain, S. Stegen, and J. Lu, "A hybrid communication platform for multi-microgrid energy management system optimization," in *International Symposium on Industrial Electronics (ISIE)*. IEEE, 2018, pp. 1215–1220.
- [22] M. Starke, A. Herron, D. King, and Y. Xue, "Implementation of a publish-subscribe protocol in microgrid islanding and resynchronization with self-discovery," *IEEE Trans. Smart Grid*, vol. 10, no. 1, pp. 361–370, 2017.
- [23] F. Girbau-Llistuella, A. Sumper, R. Gallart-Fernandez, and V. Buehner, "Operation of rural distribution grids with intermittent generation in connected and island mode using the open source EMS solver SCIP," in *International Conference on Renewable Energy Research and Applications (ICRERA)*. IEEE, 2015, pp. 983–988.
- [24] E.-K. Lee, W. Shi, R. Gadh, and W. Kim, "Design and implementation of a microgrid energy management system," *Sustainability*, vol. 8, no. 11, p. 1143, 2016.
- [25] D. E. Olivares, A. Mehrizi-Sani, A. H. Etemadi, C. A. Cañizares, R. Iravani, M. Kazerani *et al.*, "Trends in microgrid control," *IEEE Trans. Smart Grid*, vol. 5, no. 4, pp. 1905–1919, 2014.
- [26] L. Meng, E. R. Sanseverino, A. Luna, T. Dragicevic, J. C. Vasquez, and J. M. Guerrero, "Microgrid supervisory controllers and energy management systems: A literature review," *Renewable and Sustainable Energy Reviews*, vol. 60, pp. 1263–1273, 2016.
- [27] J. Almada, R. Leão, R. Sampaio, and G. Barroso, "A centralized and heuristic approach for energy management of an ac microgrid," *Renewable and Sustainable Energy Reviews*, vol. 60, pp. 1396–1404, 2016.
- [28] A. Kanwar, D. I. H. Rodríguez, J. von Appen, and M. Braun, *A Comparative Study of Optimization-and Rule-Based Control for Microgrid Operation*. Universitätsbibliothek Dortmund, 2015.
- [29] G. Kyriakarakos, A. I. Dounis, K. G. Arvanitis, and G. Papadakis, "A fuzzy logic energy management system for poly-generation microgrids," *Renewable Energy*, vol. 41, pp. 315–327, 2012.
- [30] J. Wang, C. Zhao, A. Pratt, and M. Baggü, "Design of an advanced energy management system for microgrid control using a state machine," *Applied energy*, vol. 228, pp. 2407–2421, 2018.
- [31] M. Saleh, Y. Esa, and A. Mohamed, "Centralized control for dc microgrid using finite state machine," in *IEEE Power & Energy Society Innovative Smart Grid Technologies Conference (ISGT)*, 2017, pp. 1–5.

- [32] D. E. Olivares, C. A. Cañizares, and M. Kazerani, "A centralized energy management system for isolated microgrids," *IEEE Trans. Smart Grid*, vol. 5, no. 4, pp. 1864–1875, 2014.
- [33] E. Nasr-Azadani, P. Su, W. Zheng, J. Rajda, C. Canizares, M. Kazerani *et al.*, "The Canadian Renewable Energy Laboratory: A testbed for microgrids," *IEEE Electr. Mag.*, vol. 8, no. 1, pp. 49–60, 2020.
- [34] International Organization for Standardization (ISO), "ISO/IEC 20922:2016 Information technology - Message Queuing Telemetry Transport (MQTT) v3.1.1," 2016. [Online]. Available: <https://www.iso.org/standard/69466.html>
- [35] J. Cotrell and W. Pratt, "Modeling the feasibility of using fuel cells and hydrogen internal combustion engines in remote renewable energy systems," National Renewable Energy Lab., Golden, CO.(US), Tech. Rep., 2003.
- [36] W. E. Hart, J.-P. Watson, and D. L. Woodruff, "Pyomo: modeling and solving mathematical programs in python," *Mathematical Programming Computation*, vol. 3, no. 3, pp. 219–260, 2011.
- [37] J. Forrest and R. Lougee-Heimer, "Cbc user guide," in *Emerging theory, methods, and applications*. INFORMS, 2005, pp. 257–277.
- [38] B. Meindl and M. Templ, "Analysis of commercial and free and open source solvers for linear optimization problems," Tech. Rep. ESSnet project on common tools and harmonised methodology for SDC in the ESS, 2012.
- [39] Eclipse Foundation, "Mqtt and mqtt-sn software," 2018. [Online]. Available: <http://www.eclipse.org/paho/>
- [40] Riverbank Computing, "Pyqt4 reference guide," 2016. [Online]. Available: <https://www.riverbankcomputing.com/static/Docs/PyQt4/>
- [41] K. Strunz *et al.*, "Benchmark systems for network integration of renewable and distributed energy resources," CIGRE, Tech. Rep. CIGRE Task Force C.04.02, 2013.
- [42] Cummins Power Generation Inc., "Cummins dsgaa generator set data sheet," 2011. [Online]. Available: <http://csdieselgenerators.com/Images/Generators/2117/Cumminsr-DSGAA-100-kW-spec-sheet.pdf>
- [43] Queen's Printer for Ontario, "Fuel price survey information," 2019. [Online]. Available: <https://www.ontario.ca/data/fuels-price-survey-information>
- [44] Y. Zhang, R. Wang, T. Zhang, Y. Liu, and B. Guo, "Model predictive control-based operation management for a residential microgrid with considering forecast uncertainties and demand response strategies," *IET Generation, Transmission & Distribution*, vol. 10, no. 10, pp. 2367–2378, 2016.
- [45] C.-H. Liu and J.-C. Gu, "Modeling and integrating PV stations into IEC 61850 XMPP intelligent edge computing gateway," *Energies*, vol. 12, no. 8, p. 1442, 2019.